# TOPOLOGY-AWARE HYBRID WI-FI/BLE FINGERPRINTING VIA EVIDENCE-THEORETIC FUSION AND PERSISTENT HOMOLOGY

#### A PREPRINT

Behrad Mousaei Shir-Mohammad, Behzad Moshiri and Abolfazl Yaghmaei \*† ‡

October 21, 2025

# **ABSTRACT**

Indoor localization remains challenging in GNSS-denied environments due to multipath, device heterogeneity, and volatile radio conditions. We propose a topology-aware, hybrid Wi-Fi/BLE fingerprinting framework that (i) applies physically consistent RSS normalization (dBm z-scoring or dBm $\rightarrow$ linear mW $\rightarrow$  z-score), (ii) denoises streams with classical Bayesian filters (KF/UKF/PF), (iii) combines complementary regressors (Random Forest and weighted kNN with a diagonal Mahalanobis metric), (iv) performs evidence-theoretic fusion via Dempster–Shafer theory (DST), and (v) augments each sample with persistent-homology (PH) descriptors. The system outputs both (x,y) estimates and interpretable belief maps, and is engineered for microcontroller-class deployment with per-update cost  $O(T\log M + \log M + M_p + S)$ .

We evaluate on two heterogeneous datasets—including a new 1,200-sample ESP32 survey—and report ablations, robustness to test-only noise, and significance across 10 stratified splits. Under 10% synthetic RSS noise, the full pipeline attains 3.40 m (Dataset 1) and 2.45 m (Dataset 2) RMSE, improving a strong PF+RF baseline by about 37%. Averaged across splits, it yields  $4.993 \pm 0.15$  m versus  $6.292 \pm 0.13$  m (20.6% relative reduction; p < 0.001). In noise-free tests, accuracy tightens to 0.44 m and 0.32 m (up to 56% better). Compared with recent learning-heavy approaches that assume large site-specific datasets and GPU inference, our method delivers competitive accuracy with formal uncertainty quantification and low computational cost suitable for real-time deployment.

*Keywords* Indoor localization, Wi-Fi fingerprinting, BLE beacons, Data Fusion, Discrete calculus, Kalman filter, particle filter, sensor fusion, Dempster–Shafer theory, Choquet integral, persistent homology, uncertainty quantification, embedded systems.

# 1 Introduction

Global Navigation Satellite Systems (GNSS) degrade or fail indoors, yet most buildings already host dense Wi-Fi access points and, increasingly, Bluetooth Low Energy (BLE) beacons. RSS fingerprinting leverages these ambient radios by matching received-signal-strength (RSS) vectors to a surveyed database of reference points (RPs) [1, 2]. In practice, however, multipath, device heterogeneity, and transient interference inject substantial noise into RSS, which destabilises distance metrics and degrades position estimates. Our goal is a lightweight, interpretable pipeline that explicitly addresses these realities while remaining deployable on commodity microcontrollers.

In the broader context of sensor fusion and state estimation, prior work has demonstrated the effectiveness of Kalmanfamily filters and nonlinear blending for noisy, heterogeneous sensors: GPS/INS integration with nonlinear blending filters [3], MEMS-IMU calibration with Kalman filtering [4], and robust fault handling in microgrids using the

<sup>\*</sup>Manuscript received XXXX 2025; revised XXXX 2025. This work was supported in part by the U.S. Department of Commerce under Grant BS123456.

<sup>&</sup>lt;sup>†</sup>The authors are with the School of Electrical and Computer Engineering, University of Tehran, Iran, Tehran 1439957131 (e-mail: {behrad.mousaie,yaghmaei,moshiri}@ut.ac.ir).

<sup>&</sup>lt;sup>‡</sup>All code and the dataset for this paper are available at https://github.com/behradbx/Tehran-Indoor-Localization.

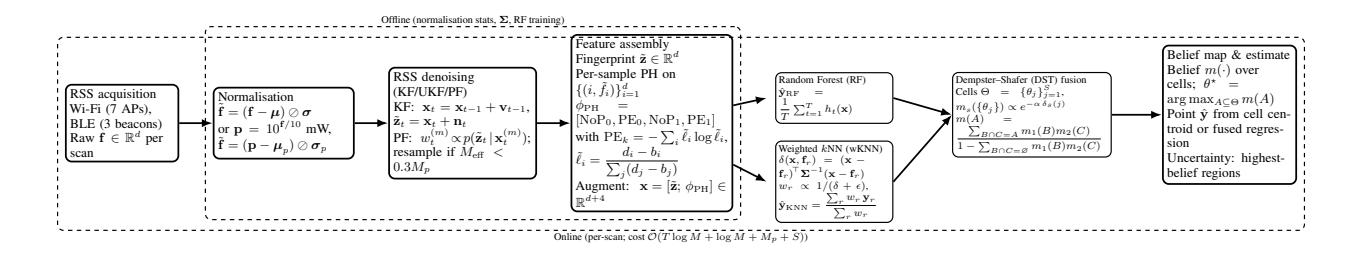


Figure 1: End-to-end hybrid Wi-Fi/BLE fingerprinting pipeline. RSS is normalised, optionally denoised (KF/UKF/PF), and augmented with per-sample persistent-homology descriptors. Two complementary regressors (RF and wKNN) produce predictions that are fused by Dempster–Shafer (DST), yielding a point estimate and an interpretable belief map. Offline: learn normalisation statistics,  $\Sigma$ , and RF. Online: per-scan operation with overall cost  $\mathcal{O}(T \log M + \log M + M_n + S)$ .

Unscented Kalman filter [5]. These results motivate our choice of KF/UKF/PF to stabilise RSS before regression, providing accuracy gains with modest computational cost.

Prior indoor-localisation work spans three strands. (i) Lightweight Wi-Fi-only methods (e.g., selective/range-limited kNN) are easy to deploy but typically plateau at several metres and rarely quantify uncertainty; for example, SLWKNN reports ~4.8 m and DumbLoc ~6.2 m in noise-free conditions, without explicit RSS noise modelling or multi-radio fusion [6, 7]. (ii) Classical learning methods improve regressors or features (e.g., RF-assisted AP selection with kernel ELM) and achieve roughly 3.9 m, but still rely on a single radio and lack uncertainty handling [8]. (iii) Learning-heavy models learn complex radio-environment mappings and can reach 1-2 m using CNN-LSTM or high-order GNNs [9, 14]; extensions with data augmentation and temporal modelling further push accuracy, e.g., CSI trajectory fingerprinting with GAN-augmented CNN-LSTM [10] and generative hidden-Markov Wi-Fi fingerprinting attaining sub-meter accuracy under controlled conditions [11]. In parallel, Xia et al. optimise RSSI fingerprint matching in wireless sensor networks by refining the matching scheme for efficiency and accuracy [12]. While effective, these approaches are *single-modality* and typically do not expose uncertainty or perform evidence-theoretic fusion; by contrast, our hybrid Wi-Fi+BLE design integrates DST/Choquet fusion and PH features, and targets microcontroller-class deployment. Hybrid sensing has also been explored: SPOTTER fuses Wi-Fi and BLE in a particle-filter framework and reports  $\sim$ 2.7 m, but with comparatively heavy computation and without demonstration on resource-constrained hardware [13]. Complementary studies of multi-sensor fusion show that Dempster-Shafer evidence theory is effective under conflicting/uncertain measurements, and fuzzy aggregation can capture non-linear complementarity [22, 23]. These gaps motivate a solution that pairs multi-modal sensing and principled fusion with efficient, classical components.

We therefore propose a lightweight, real-time hybrid Wi-Fi/BLE fingerprinting framework that integrates four components: (i) RSS filtering via Kalman, Unscented Kalman, or Particle filters to attenuate fast fading [18]; (ii) dual regressors—Random Forest (RF) and weighted *k*-nearest neighbours (wKNN)—to produce complementary coordinate predictions; (iii) model fusion using Dempster–Shafer Theory (DST) for principled evidence combination and a two-source Choquet fuzzy integral to capture non-linear complementarity [19, 20]; and (iv) topology-aware features computed *per sample* via persistent homology (PH) to summarise channel-structure geometry beyond variance-based statistics [21]. DST yields spatial belief maps visualised as highest-belief regions rather than Gaussian ellipses, improving operator interpretability. RF and wKNN respond differently to noise and RP sparsity, so fusing them stabilises predictions across sites; filtering reduces measurement noise at the source; and PH descriptors capture coarse geometric structure that PCA-like features may miss. All components are commodity, require no GPUs, and suit embedded deployment. Our design is informed by successes of nonlinear Kalman filtering and fuzzy aggregation in related sensing domains [3–5, 22, 23].

#### **Problem Statement and Notation**

We consider indoor fingerprinting on a bounded floor plan. At time t, the sensor acquires a Wi-Fi/BLE RSS vector  $\mathbf{f}_t \in \mathbb{R}^d$  across  $N_W$  Wi-Fi and  $N_B$  BLE channels  $(d = N_W + N_B)$ . Let  $\mathcal{D}_{\text{train}} = \{(\mathbf{f}^{(n)}, \mathbf{r}^{(n)})\}_{n=1}^M$  be the labelled fingerprint-location pairs at surveyed reference points (RPs), with  $\mathbf{r}^{(n)} = (x^{(n)}, y^{(n)}) \in \mathbb{R}^2$ . The goal is to estimate  $\hat{\mathbf{r}}_t = (\hat{x}_t, \hat{y}_t)$  for a new  $\mathbf{f}_t$ , while also exposing spatial uncertainty via a belief map over discretised cells  $\Theta = \{\theta_j\}_{j=1}^S$ .

We normalise fingerprints either in dBm (direct z-score) or via dBm $\rightarrow$ linear power (mW) $\rightarrow$  z-score (Sec. 2.1). For denoising, we apply KF/UKF/PF to the *per-feature* temporal stream (Sec. 2.3). Two complementary regressors—RF and variance-weighted wKNN—produce coordinate predictions (Sec. 2.2), which are fused by Dempster–Shafer theory

(DST) on  $\Theta$ ; a two-source Choquet integral aggregates confidences (Sec. 2.4). We optionally augment each input with four persistent-homology (PH) descriptors computed on the 1-D embedded curve of the normalised fingerprint (Sec. 2.5).

#### **Contributions**

- A unified, compute-efficient Wi-Fi/BLE fingerprinting pipeline combining classical filtering, complementary regressors, evidence-theoretic fusion, and per-sample PH features—producing both point estimates and interpretable belief maps [19, 21].
- A physically meaningful feature normalisation: either direct z-scoring in dBm or dBm→linear power (mW)→
  z-score; we avoid ln | · | on dBm, which lacks physical meaning.
- A transparent per-update complexity of  $O(T \log M + \log M + M_p + S)$  for T trees (RF), M training fingerprints,  $M_p$  PF particles (if enabled), and S spatial cells for DST—consistent with real-time use on microcontroller-class processors.
- A comprehensive evaluation on two heterogeneous datasets—including a new 1,200-sample ESP32 survey—and ablations isolating each module under both noise-free and 10% synthetic-noise conditions [15].

**Results in brief** Under the unified 10% noise definition (Sec. 3.2), the full pipeline attains 3.40 m (Dataset 1) and 2.45 m (Dataset 2) RMSE on the canonical held-out split, improving over a strong PF+RF baseline by about 37%. In noise-free conditions, accuracy tightens to 0.44 m and 0.32 m, up to 56% better than the same baseline. Averaged across 10 stratified splits with the same 10% noise, the mean RMSE is  $4.993 \pm 0.15$  m versus  $6.292 \pm 0.13$  m for PF+RF (20.6% reduction; Table 4). This explains why Table 3 (canonical split) and Table 4 (10-split average) report different absolute values under the same noise setting.

Scope and fairness Where many deep models assume site-specific large training sets and GPU-class compute [9–11, 14], our focus is robust performance on commodity radios and embedded hardware. We report both noisy and noise-free results and clearly distinguish them (several comparative works publish only noise-free figures [6–8]). Uncertainty is reported as belief maps via DST [19].

**Paper organization** Section 2 presents the full pipeline—normalisation, RSS filtering, regression, fusion, and persample PH features—together with a brief complexity analysis. Section 3 describes the datasets and protocol, reports ablations and statistical tests, and benchmarks against recent work. Section 4 summarises the findings and outlines future directions.

# 2 Proposed Methodology

The proposed hybrid Wi-Fi/BLE framework comprises an *offline* fingerprint—map construction stage and an *online* real-time positioning stage. Figure 1 gives a high-level view of the pipeline; details follow.

#### 2.1 Data Collection and Pre-processing

Environments and datasets. Two heterogeneous datasets are used. Dataset 1 was collected on the third floor of the Faculty of Electrical and Computer Engineering, University of Tehran (see Fig. 3). We surveyed 15 reference points (RPs) distributed over a  $6 \, \text{m} \times 14 \, \text{m}$  area (not a  $50 \, \text{cm}$  lattice). At each RP we recorded RSS from 7 Wi-Fi APs and 3 BLE beacons using commodity ESP32 boards (one scanning Wi-Fi, one BLE). To reduce fast fading, we aggregate consecutive windows of 10 scans into a single fingerprint; across the site this yields 1,200 fingerprints (80 windowed fingerprints per RP). Dataset 2 [15] contains 16 RPs with 5 Wi-Fi and 3 BLE channels and 1,400 fingerprints, built with the same windowing rule.

Fingerprint vector and normalisation. Let  $N_W$  and  $N_B$  denote the numbers of Wi-Fi and BLE channels. The fingerprint at RP r is

$$\mathbf{f}_r = \left[ \rho_r^{(1)}, \dots, \rho_r^{(N_W)}, \ \beta_r^{(1)}, \dots, \beta_r^{(N_B)} \right]^\top \in \mathbb{R}^d$$
 (1)

$$d = N_W + N_B. (2)$$

We avoid applying  $\ln |\cdot|$  to dBm values (not physically meaningful). Instead, we use one of two physically consistent normalisations: (i) direct z-scoring in dBm with statistics from the training set,

$$\tilde{\mathbf{f}}_r = (\mathbf{f}_r - \boldsymbol{\mu}) \oslash \boldsymbol{\sigma},\tag{3}$$

or (ii) conversion to linear power before z-scoring,

$$\mathbf{p}_r = 10^{\mathbf{f}_r/10} \text{ (mW)}, \qquad \tilde{\mathbf{f}}_r = (\mathbf{p}_r - \boldsymbol{\mu}_p) \oslash \boldsymbol{\sigma}_p.$$
 (4)

Unless stated otherwise we adopt the dBm z-score variant. The same statistics are applied to validation/test data.

At each RP we collected raw scans at a fixed sampling cadence and averaged consecutive windows of 10 scans into a single fingerprint (80 fingerprints per RP on Dataset 1). The device height/pose and human presence were kept consistent across RPs to reduce occlusion bias; scans were performed in multiple short sessions to mitigate temporal drift. All normalisation statistics  $(\mu, \sigma \text{ or } \mu_p, \sigma_p)$  are estimated *on training data only* and reused for validation/test to prevent leakage.

# 2.2 Regression Models

We considered Linear Regression, SVR (RBF), Decision Tree, Random Forest (RF), and weighted kNN (wKNN). Hyper-parameters are tuned by five-fold cross-validation; the final ensemble retains **RF** and **wKNN** as complementary predictors that map  $\tilde{\mathbf{f}}$  to 2-D coordinates  $\hat{\mathbf{r}} = (\hat{x}, \hat{y})$ .

**Distance metric for wKNN.** During prediction, we use a diagonal Mahalanobis-type distance in fingerprint space to equalise Wi-Fi/BLE dimensions:

$$\delta(\tilde{\mathbf{z}}, \tilde{\mathbf{f}}_r) = (\tilde{\mathbf{z}} - \tilde{\mathbf{f}}_r)^{\top} \mathbf{\Sigma}^{-1} (\tilde{\mathbf{z}} - \tilde{\mathbf{f}}_r), \tag{5}$$

where  $\Sigma = \operatorname{diag}(\hat{\sigma}_1^2, \dots, \hat{\sigma}_d^2)$  are channel-wise variances estimated on the training set with  $\ell_2$ -shrinkage ( $10^{-6}$  added to the diagonal) for numerical stability. wKNN uses inverse-distance weights; RF follows standard bagging over T trees.

Channel variances differ across Wi-Fi and BLE; scaling by  $\Sigma = \operatorname{diag}(\hat{\sigma}_1^2, \dots, \hat{\sigma}_d^2)$  equalises dimensions and reduces dominance by a few volatile channels. We estimate  $\hat{\sigma}_i^2$  on the *training set* with  $\ell_2$ -shrinkage (+10<sup>-6</sup>) to improve conditioning, then keep  $\Sigma$  fixed at test time.

## 2.3 RSS Noise Filtering

Filtering is applied independently per RSS channel (scalar states), which is sufficient in our setting and reduces computational burden. For KF/UKF we set the measurement variance of channel i to  $R_i = \hat{\sigma}_i^2$  from the training set, and choose  $Q_i = \gamma R_i$  with  $\gamma \in \{0.25, 0.5, 1\}$  (Table 1). For PF, the likelihood uses the same  $R_i$  and a unit-variance random walk in prediction; effective-sample-size (ESS) triggers systematic resampling (Alg. 1).

Instantaneous RSS vectors  $\tilde{\mathbf{z}}_t$  are smoothed prior to regression using classical Bayesian filters [18]:

- 1. Kalman Filter (KF): linear-Gaussian state  $\mathbf{x}_t = \mathbf{x}_{t-1} + \mathbf{v}_{t-1}, \ \tilde{\mathbf{z}}_t = \mathbf{x}_t + \mathbf{n}_t$ , with  $\mathbf{v}_{t-1} \sim \mathcal{N}(\mathbf{0}, \mathbf{Q})$  and  $\mathbf{n}_t \sim \mathcal{N}(\mathbf{0}, \mathbf{R})$ .
- 2. Unscented KF (UKF): sigma-point prediction to handle mild non-linearities.
- 3. **Particle Filter (PF):** non-parametric recursion with  $M_p$  particles  $\{(\mathbf{x}_t^{(m)}, w_t^{(m)})\}_{m=1}^{M_p}$ ; resampling occurs when  $\mathrm{ESS} = 1/\sum_m (w_t^{(m)})^2 < \tau M_p$ .

PF attained the lowest error in our experiments; KF provides a favourable accuracy/latency trade-off for embedded deployment.

#### 2.4 Multi-Model Fusion and Uncertainty

**DST grid and distance mapping.** We tile the floor with square cells of width  $h \in \{0.5, 0.75, 1.0\}$  m (Table 1). Each regressor s outputs a point estimate  $\hat{\mathbf{r}}_s$ ; we compute distances to cell centroids  $\delta_s(j) = \|\hat{\mathbf{r}}_s - \mathbf{c}_j\|_2^2$  and convert them to singleton masses via Eq. (5) with scale  $\alpha$ . Smaller h increases S and yields finer belief maps at a modest O(S) runtime cost (Eq. (12)).

Confidence scores for Choquet. We define per-regressor confidences as  $s_s = \max_j c_s(j)$  with  $c_s(j) = \exp\{-\beta \delta_s(j)\}$ , where  $\beta$  is set to the inverse of the median validation-set distance (per dataset). This yields  $s_s \in [0,1]$  that increases as the predicted point aligns tightly with a few high-belief cells.

We fuse RF and wKNN predictions and quantify uncertainty using Dempster–Shafer Theory (DST) [19] and a two-source Choquet fuzzy integral [20].

**Dempster–Shafer evidence fusion.** Discretise the environment into S cells with centers  $\{\mathbf{c}_j\}_{j=1}^S$  and frame of discernment  $\Theta = \{\theta_1, \dots, \theta_S\}$ . Each regressor  $s \in \{\text{RF}, \text{KNN}\}$  yields a point estimate  $\hat{\mathbf{r}}_s$  and induces a basic-belief assignment (BBA)  $m_s : 2^\Theta \to [0, 1]$  by mapping distances to singleton masses:

$$\delta_s(j) = \|\hat{\mathbf{r}}_s - \mathbf{c}_j\|_2, \qquad m_s(\{\theta_j\}) = \frac{\exp(-\alpha \,\delta_s(j))}{\sum_{i=1}^S \exp(-\alpha \,\delta_s(i))}, \tag{6}$$

$$m_s(\Theta) = 1 - \sum_{j=1}^{S} m_s(\{\theta_j\}),$$
 (7)

with scale  $\alpha > 0$ . The fused mass  $m(\cdot)$  is obtained by Dempster's rule

$$m(A) = \frac{\sum_{B \cap C = A} m_{\text{RF}}(B) m_{\text{KNN}}(C)}{1 - \sum_{B \cap C = \varnothing} m_{\text{RF}}(B) m_{\text{KNN}}(C)}.$$
(8)

We estimate the location as the cell of maximum singleton belief  $\theta^* = \arg \max_j m(\{\theta_j\})$  and also visualise belief maps for operator interpretability.

Choquet fuzzy integral. Let  $s_1, s_2 \in [0, 1]$  be normalised confidence scores (higher is better) from RF and wKNN. A fuzzy measure  $\mu$  on  $\Omega = \{\omega_1, \omega_2\}$  satisfies  $\mu(\emptyset) = 0$ ,  $\mu(\Omega) = 1$ , and monotonicity  $\mu(\{\omega_i\}) \in [0, 1]$ ,  $\max\{\mu(\{\omega_1\}), \mu(\{\omega_2\})\} \le 1$  [20]. For two sources, the Choquet integral has the closed form

$$C_{\mu}(s_1, s_2) = s_{(1)} \,\mu(\Omega) + \left(s_{(2)} - s_{(1)}\right) \,\mu\left(\left\{\omega_{(2)}\right\}\right),\tag{9}$$

where  $s_{(1)} \le s_{(2)}$  are the ordered scores. We learn  $\mu(\{\omega_1\})$  and  $\mu(\{\omega_2\})$  on the validation set by least squares under  $0 \le \mu(\{\omega_i\}) \le 1$ .

# 2.5 Topology-Aware Features via Persistent Homology

To enrich each fingerprint with geometry-aware descriptors, we compute *per-sample* persistent-homology (PH) features so that they are available at test time without re-running dataset-level analyses [21]. Given a normalised fingerprint  $\tilde{\mathbf{f}} \in \mathbb{R}^d$ , we embed it as a 1-D point cloud

$$\mathcal{X} = \{(i, \tilde{f}_i)\}_{i=1}^d \subset \mathbb{R}^2,\tag{10}$$

and run a Vietoris–Rips filtration to obtain persistence diagrams for  $H_0$  and  $H_1$ . From each diagram we extract two summaries:

$$NoP_k = N_k, (11)$$

$$PE_k = -\sum_{i=1}^{N_k} \tilde{\ell}_i \log \tilde{\ell}_i, \qquad \tilde{\ell}_i = \frac{d_i - b_i}{\sum_j (d_j - b_j)},$$
(12)

where  $(b_i, d_i)$  are birth-death pairs and  $k \in \{0, 1\}$ . The four scalars  $[\text{NoP}_0, \text{PE}_0, \text{NoP}_1, \text{PE}_1]$  are concatenated to  $\tilde{\mathbf{f}}$  before regression. Empirically,  $H_0$  carries most of the signal;  $H_1$  is often small but retained for completeness.

We compute VR-based PH descriptors with giotto-tda (default radius schedule) on the 1-D embedded curve  $\{(i, \tilde{f}_i)\}_{i=1}^d$ . For  $d \leq 16$ , per-sample wall-clock is < 1 ms on a laptop-class CPU; features are z-scored and concatenated to  $\tilde{\mathbf{f}}$ . In ablations,  $H_0$  carries most signal; we retain  $H_1$  for completeness (Sec. 3.6).

# 2.6 Complexity Analysis

For one query, the dominant costs are:

- RF prediction:  $O(T \cdot \text{depth})$  with depth  $\approx \log M$  for M training points in balanced trees;
- wKNN search:  $O(\log M)$  average with a kd-tree (degrading toward O(M) as d grows);
- Filtering: KF/UKF O(1) per step in our setting; PF  $O(M_p)$  for  $M_p$  particles;
- Fusion (DST): O(S) for S spatial cells.

Overall, per-update complexity is approximately

$$O(T\log M + \log M + M_p + S), \tag{13}$$

compatible with real-time execution on microcontroller-class hardware.

Component	Symbol	Grid / Rule	Notes
wKNN	k	{3,5,7,9}	Choose <i>k</i> minimizing CV-RMSE.
wKNN metric	$oldsymbol{\Sigma}$	Diagonal variances with $\ell_2$ -shrinkage $10^{-6}$	As in Sec. 2.2.
RF	T	$\{100, 200, 400\}$	Bootstrap; max_features = $\sqrt{d}$ .
RF	max_depth	{16, 24, 28, None}	Early stop by leaf purity if None.
KF/UKF	$\mathbf{Q},\mathbf{R}$	$\mathbf{R} = \operatorname{diag}(\hat{\sigma}_1^2, \dots, \hat{\sigma}_d^2); \mathbf{Q} = \gamma \mathbf{R},$	Pick $\gamma$ by CV.
		$\gamma \in \{0.25, 0.5, 1\}$	
PF	$M_p$	$5 \times 10^3, 10^4, 2 \times 10^4$	Resample if ESS $< \tau M_p, \tau \in \{0.3, 0.5\}.$
DST	$\alpha$	0.1, 0.2, 0.5, 1, 2, 5	Minimizes validation RMSE of fused estimate.
DST grid	S cells	Cell width $h \in \{0.5, 0.75, 1.0\} \mathrm{m}$	$S = \lceil \operatorname{area}/h^2 \rceil.$
Choquet	$\mu(\{\omega_1\}), \mu(\{\omega_2\})$	LS fit on validation set, $0 \le \mu(\{\omega_i\}) \le 1$	Monotone measure, $\mu(\Omega) = 1$ .
PH	VR radius	Library default	See Sec. 2.7.

Table 1: Key hyper-parameters, search grids, and selection rules.

# 2.7 Implementation Details, Hyper-parameters, and Sensitivity

This section fixes all tunable choices and reports how they are selected. Unless noted otherwise, all statistics (means/variances for normalisation, filter covariances, cross-validation splits) are computed on the training set only and reused for validation/test.

## Hyper-parameter selection protocol

We use five-fold cross-validation on the training set to pick hyper-parameters, with a small grid per component and RMSE as the criterion. The final model is refit on the union of the five folds with the selected values and evaluated on the held-out test set. Randomised procedures (RF bootstraps, PF particles, train/validation splits) use fixed seeds for reproducibility.

#### Noise models and robustness tests

We evaluate robustness under two realistic perturbations applied at test time to the normalised RSS vector  $\tilde{\mathbf{z}}$ :

(i) Gaussian jitter with level  $\eta \in \{0.05, 0.10, 0.20\}$ :

$$\tilde{z}_i' = \tilde{z}_i + \eta \,\hat{\sigma}_i \,\epsilon_i, \quad \epsilon_i \sim \mathcal{N}(0, 1).$$
 (14)

(ii) Bursty outliers with probability  $p \in \{0.02, 0.05\}$  per channel:

$$\tilde{z}_i' = \begin{cases} \tilde{z}_i + \kappa \, \hat{\sigma}_i \, u, & \text{with prob. } p, \ u \sim \text{Laplace}(0, 1), \\ \tilde{z}_i, & \text{otherwise,} \end{cases}$$
 (15)

with  $\kappa \in \{2, 3\}$ . We report RMSE degradation relative to the clean case and perform paired Wilcoxon signed-rank tests across test samples, Holm–Bonferroni corrected, to assess significance ( $\alpha = 0.05$ ).

# **DST** configuration and confidences

We discretise the floor plan into S cells using square cells of width h (Table 1). For each regressor  $s \in \{RF, KNN\}$  we turn distance scores into singleton masses as above with scale  $\alpha$ . To produce the two confidence scores  $s_1, s_2$  used by the Choquet integral, we map distances to [0, 1] via

$$c_s(j) = \exp\{-\beta \,\delta_s(j)\}, \qquad s_s = \max_j c_s(j), \tag{16}$$

where  $\beta$  is set to the inverse of the median  $\delta_s(j)$  over the validation set (per dataset). As a baseline ablation, we also report a simple convex combination  $\hat{\mathbf{r}} = \lambda \, \hat{\mathbf{r}}_{\mathrm{RF}} + (1 - \lambda) \, \hat{\mathbf{r}}_{\mathrm{KNN}}$  with  $\lambda \in \{0.25, 0.5, 0.75\}$ ; the main results use full DST (Eq. 8).

# Persistent-homology implementation and cost

We compute per-sample PH features with giotto-tda (Vietoris-Rips) on the point cloud  $\mathcal{X} = \{(i, \tilde{f}_i)\}_{i=1}^d$  (Sec. 2.5), extracting [NoP<sub>0</sub>, PE<sub>0</sub>, NoP<sub>1</sub>, PE<sub>1</sub>]. For our 1D embedded curves the VR filtration builds  $O(d^2)$  edges; wall-clock is

# Algorithm 1 Particle filtering per feature with systematic resampling

```
Require: measurements \{z_t\}_{t=1}^T, particles M_p, noise variance R, threshold \tau

1: Init: x_0^{(m)} \sim \mathcal{N}(0,1), w_0^{(m)} = 1/M_p

2: for t=1 to T do

3: Predict: x_t^{(m)} \leftarrow x_{t-1}^{(m)} + \varepsilon^{(m)}, \ \varepsilon^{(m)} \sim \mathcal{N}(0,\sigma^2)

4: Update: w_t^{(m)} \leftarrow w_{t-1}^{(m)} \exp\left(-\frac{(x_t^{(m)}-z_t)^2}{2R}\right)

5: Normalize: w_t^{(m)} \leftarrow w_t^{(m)}/\sum_j w_t^{(j)}

6: if ESS = 1/\sum_m (w_t^{(m)})^2 < \tau M_p then

7: Systematic\ resampling:\ draw\ indices\ \{i_m\}_{m=1}^{M_p}

8: x_t^{(m)} \leftarrow x_t^{(i_m)}, \ w_t^{(m)} \leftarrow 1/M_p

9: end if

10: Output: \hat{x}_t = \sum_m w_t^{(m)} x_t^{(m)}

11: end for
```

< 1 ms per sample for  $d \le 16$  on a laptop-class CPU (measured once and amortised offline to precompute features for training; at test time these four scalars are computed on-the-fly). Features are z-scored and concatenated to  $\tilde{\mathbf{f}}$ ; we verified that adding only  $H_0$  yields almost identical accuracy, but we retain  $H_1$  for completeness.

# Filtering choices and measurement covariances

For KF/UKF we set  $\mathbf{R}$  to the diagonal of empirical channel variances from the training set and choose  $\mathbf{Q} = \gamma \mathbf{R}$  with  $\gamma$  from Table 1. The PF uses a random-walk state model per feature, importance weights from the Gaussian likelihood with variance R (the scalar counterpart of  $\mathbf{R}$ ), and systematic resampling when the effective sample size  $\mathrm{ESS} = 1/\sum_{m} (w_t^{(m)})^2$  falls below  $\tau M_p$ .

#### Sensitivity reporting and statistics

We provide one-parameter sweeps for k, T,  $M_p$ ,  $\alpha$ , and h around their selected values and report (i) mean  $\pm$  std. RMSE across test samples; (ii) relative change vs. the default model; and (iii) paired Wilcoxon p-values against the default. All tables clearly separate noise-free and noisy settings [Eqs. (14)–(15)].

# Reproducibility checklist

We release code with: fixed seeds, exact grids in Table 1, scripts for PH feature extraction, filter calibration, and fusion ablations; and JSON files storing  $\mu$ ,  $\sigma$ ,  $\Sigma$ ,  $\Omega$ ,  $\Omega$ , and  $(\mu(\{\omega_i\}))$  for each dataset.

#### 2.8 Summary

We proposed a hybrid Wi-Fi/BLE indoor localization pipeline that combines: (i) physically consistent normalization (dBm z-score baseline); (ii) temporal denoising via KF/UKF/PF with data-driven covariances and ESS-based systematic resampling; (iii) complementary regressors (RF and variance-weighted wKNN with a diagonal Mahalanobis metric); (iv) principled fusion via Dempster–Shafer evidence on a discretized floor plan and a learned two-source Choquet integral for confidences; and (v) per-sample, topology-aware features from persistent homology (giotto-tda). Implementation details and all hyper-parameters (RF trees/depth, KNN k and metric, PF particles/threshold, DST scale  $\alpha$  and cell width k, Choquet measure) are selected by five-fold cross-validation and listed in Table 1; Algorithm 1 specifies the PF step. Robustness is evaluated under Gaussian jitter and bursty outliers (Eqs. 14–15), and we report sensitivity curves with non-parametric significance tests. This modular design yields accurate point estimates with interpretable belief maps while remaining lightweight for embedded deployment [18, 19, 21].

# 3 Experimental Evaluation and Results

This section details datasets and hardware, the evaluation protocol and metrics, ablation studies, robustness to synthetic noise, significance tests across splits, runtime on embedded hardware, and a comparison against recent literature.



Figure 2: Real picture of Test area for Dataset 1 on the third floor of the Faculty of Electrical and Computer Engineering, University of Tehran.

# 3.1 Datasets and Hardware

**Dataset 1** comprises 15 RPs in a  $6 \times 14$  m area, with RSS from 7 Wi-Fi APs and 3 BLE beacons. Consecutive windows of 10 scans are averaged into single fingerprints, yielding 1,200 fingerprints (80 per RP). **Dataset 2** (industrial environment) provides 16 RPs with 5 Wi-Fi and 3 BLE channels and 1,400 fingerprints, built with the same windowing rule [15]. Data were acquired using commodity ESP32 boards.

## 3.2 Protocol and Metrics

We adopt a stratified split by RP with a 70:15:15 train/validation/test division on both datasets. Unless stated, fingerprints are normalised via dBm z-scoring (Section 2.1). The regression ensemble uses Random Forest (RF; T=200, depth 28) and weighted kNN (wKNN; k=7, inverse-distance weights). RSS streams are optionally smoothed with KF, UKF, or PF ( $M_p$ =10<sup>4</sup>).

**Metric.** We report Euclidean  $RMSE_{xy}$  (metres) on the held-out test set, both *noise-free* and under 10% synthetic Gaussian noise injected into RSSI prior to filtering.

Noise model and reproducibility (used throughout). For noisy results we inject *test-only*, zero-mean Gaussian perturbations in dBm. For channel i we add  $\varepsilon_i \sim \mathcal{N}(0, (0.10\,\sigma_i)^2)$  to the raw RSSI before filtering and normalisation, where  $\sigma_i$  is the *training-set* standard deviation of channel i (in dBm). Unless noted, we use a fixed random seed (e.g., 123) for reproducibility. This definition is used consistently in all figures and tables that reference "10% noise." For statistical robustness we repeat the full protocol over 10 random stratified splits and report 95% confidence intervals.

## 3.3 Effect of Regressors

RF consistently achieves the lowest RMSE (Figs. 4a–4b), while wKNN provides complementary strengths on locally smooth regions of the fingerprint space. This motivates fusing both predictors downstream.

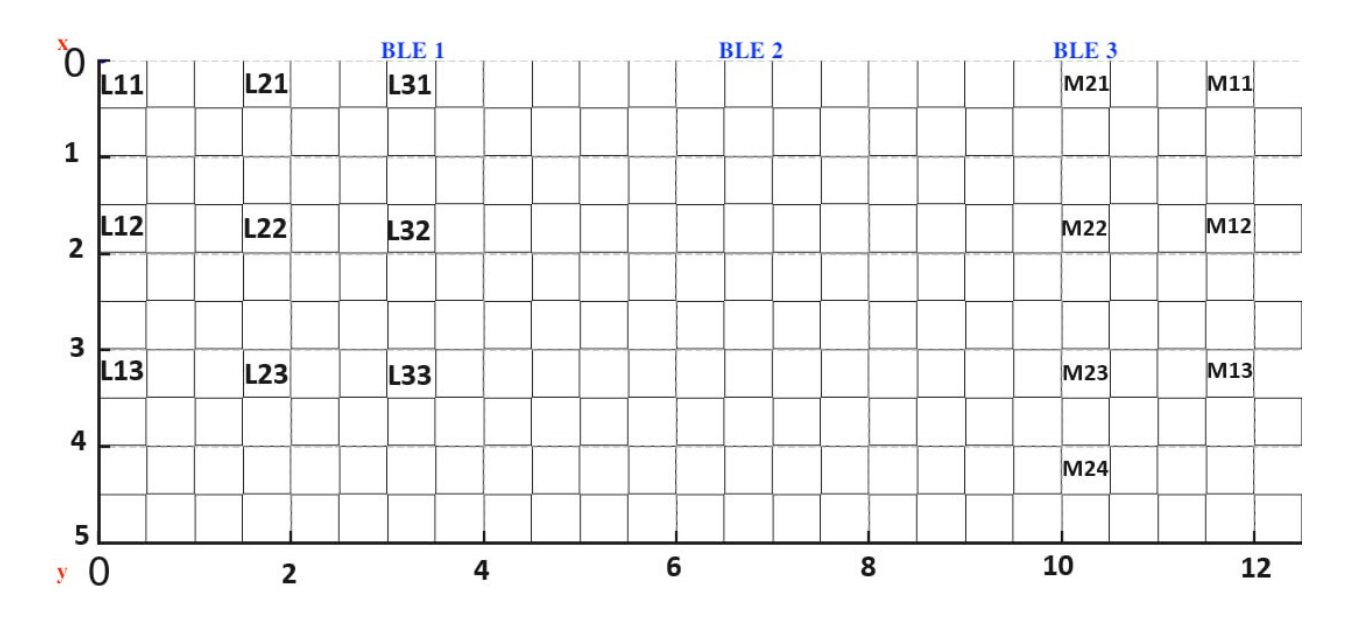


Figure 3: Map of Test area for Dataset 1 on the third floor of the Faculty of Electrical and Computer Engineering, University of Tehran. Fifteen reference points are distributed across a  $6 \text{ m} \times 14 \text{ m}$  area (50 cm each lattice).

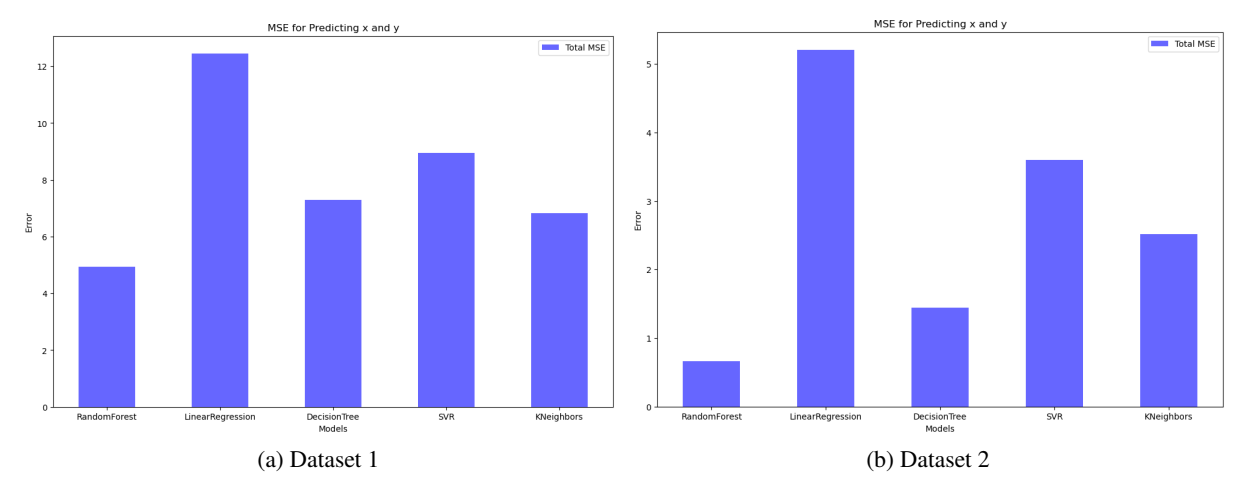


Figure 4: Regressor comparison (noise-free). RF attains the best overall accuracy; wKNN is second due to strong local interpolation. Linear models and single trees underperform; the ranking is consistent across both datasets.

# 3.4 RSS Noise Filtering

PF yields the lowest error across sites (Figs. 5a, 5b) but increases latency substantially (Figs. 5c, 5d). For embedded deployments we therefore report KF as the default real-time configuration and PF as an accuracy-optimised variant.

#### 3.5 Fusion of RF and wKNN

DST fuses disagreeing predictors by redistributing conflict mass, yielding small but consistent accuracy improvements over Choquet (Figs. 6a–6d).

# 3.6 Topology-Aware Features (PH)

PH features provide a *modest* stand-alone gain relative to PF+RF (typically  $\leq 1\%$  across our splits), but when combined with *fusion* (PF+PH+RF+wKNN+DST) they contribute to the best overall accuracy (Sections 3.7–3.8). Fig. 8 shows

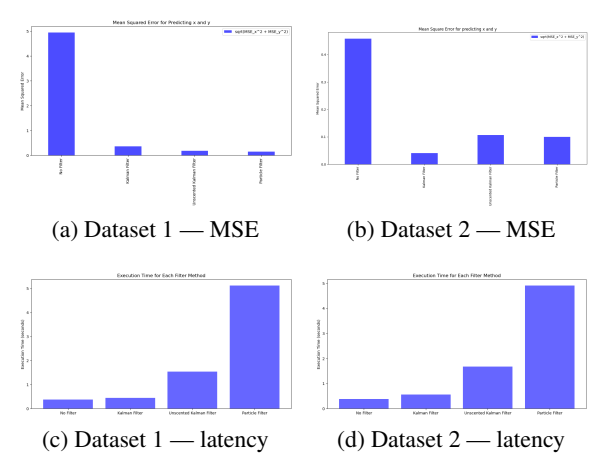


Figure 5: Filter accuracy/latency trade-offs. Particle filtering (PF) yields the lowest error but at a higher computational cost; Kalman filtering (KF) offers the best real-time compromise. Trends are consistent across both datasets.

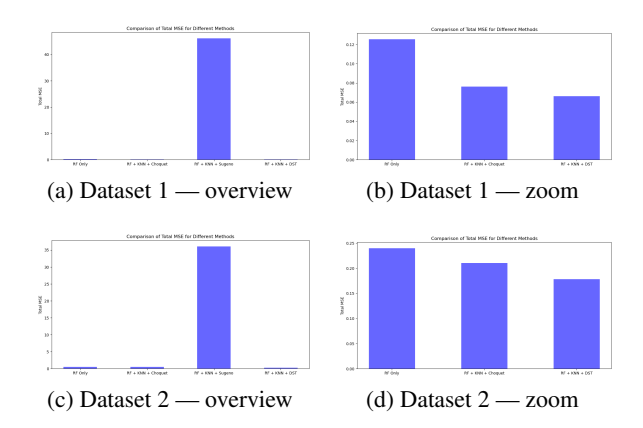


Figure 6: Fusion of RF and wKNN. Dempster–Shafer (DST) provides the strongest gains on both datasets; the Choquet integral captures non-linear complementarity but is marginally weaker.

that replacing PH by two PCA components yields smaller gains, indicating that homological summaries encode complementary, scale-invariant structure.

#### 3.7 Noise-Free Baseline Comparison

Without injected noise, the PF+RF baseline achieves  $\sim 1.0$  m (D1) and 0.68 m (D2). Evidence-theoretic fusion alone reduces error by  $\approx 20-23\%$ , and adding PH tightens it further to 0.44 m / 0.32 m (Table 2).

# 3.8 Robustness to Synthetic Noise (10%)

Under 10% noise, fusion plus PH yields the largest resilience margin, improving over PF+RF by  $\approx$ 37% on average (Table 3). Figures 10–11 show that each module (Filtering  $\rightarrow$  Fusion  $\rightarrow$  PH) incrementally suppresses the impact of noise.

# 3.9 Statistical Significance Across Splits

Across ten stratified splits, the full pipeline achieves  $4.993 \pm 0.15$  m versus  $6.292 \pm 0.13$  m for PF+RF (Table 4), a **20.6**% relative reduction. Both a paired t-test and a Wilcoxon signed-rank test yield p < 0.001, confirming statistical significance.

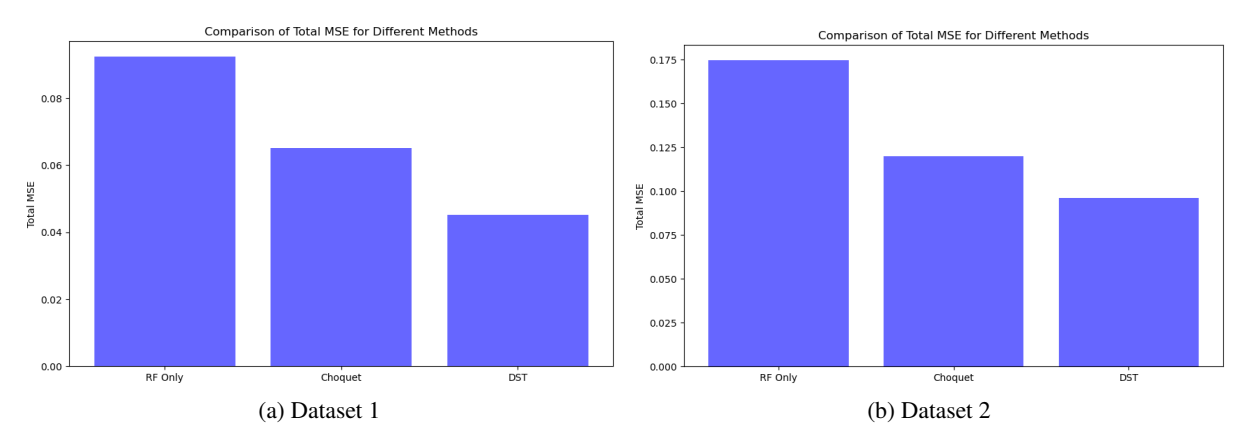


Figure 7: Persistent-homology (PH) feature ablation. Dataset 1 (left) and Dataset 2 (right) show similar trends.

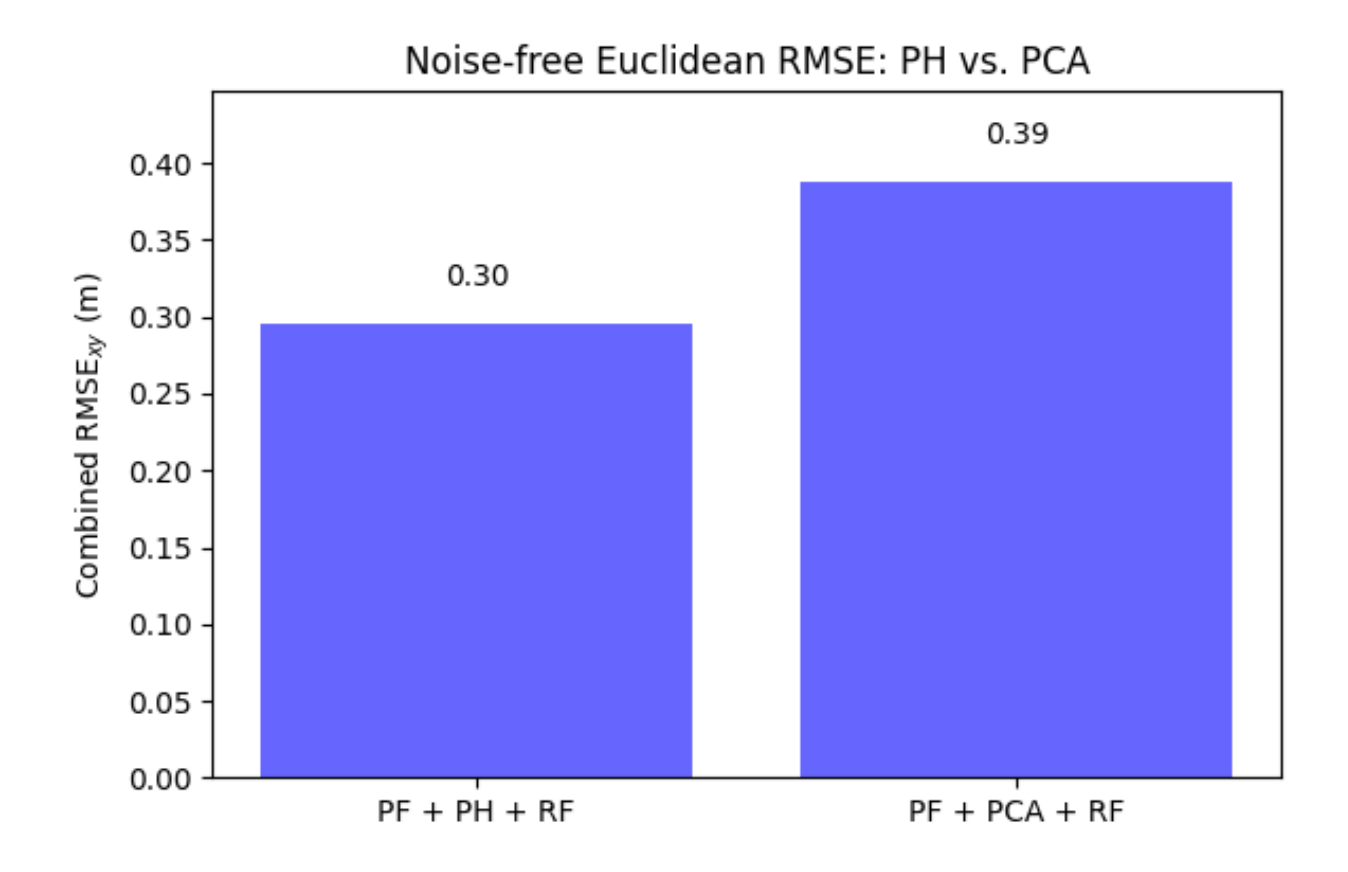


Figure 8: Noise-free  $\mathrm{RMSE}_{xy}$  on Dataset 1 when PH descriptors are replaced by two PCA components. PH provides complementary, non-linear structure beyond variance capture.

## 3.10 Runtime

The KF variant runs in real time on ESP32-class microcontrollers (Fig. 12). Enabling PF improves accuracy but increases latency substantially; practitioners can choose per deployment constraints.

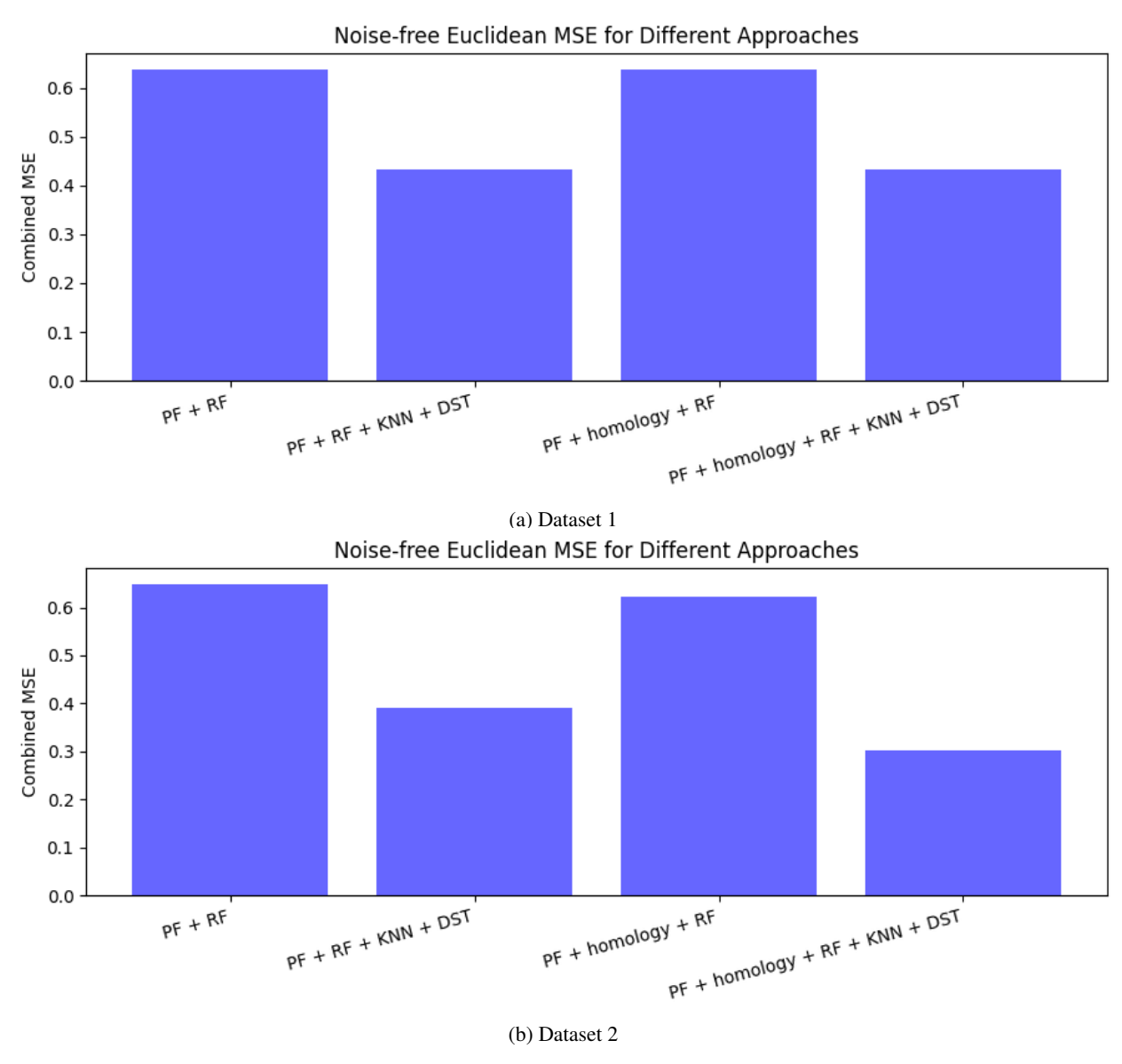


Figure 9: Noise-free  $\mathrm{RMSE}_{xy}$  across pipeline variants for both datasets.

## 3.11 Comparison with Recent Literature

Lightweight Wi-Fi-only baselines (RLWKNN, DumbLoc) deliver 4–6 m errors under noise-free evaluation, while our hybrid Wi-Fi+BLE pipeline reaches 0.44 m / 0.32 m in noise-free conditions (Table 2). Against deep models (HoGNNLoc, DLoc), our system offers competitive accuracy when accounting for *compute and training footprint*: deep methods assume large site-specific datasets and GPU inference, whereas our pipeline uses commodity radios and runs on microcontrollers. Under deliberately degraded conditions (10% noise), our method maintains 3.40 m / 2.45 m — demonstrating robustness that many prior works do not report. In short, *our gains arise from (i) multi-radio sensing, (ii) complementary regressors, (iii) evidence-theoretic fusion, and (iv) topology-aware features*, rather than heavy neural models.

## 3.12 Discussion and Takeaways

The results support three takeaways: (1) *Filtering matters*, PF offers the best accuracy, while KF enables real-time embedded operation; (2) *Fusion matters*, DST consistently improves over individual regressors and over Choquet on our datasets; (3) *Topology helps*, PH alone is a modest gain, but it synergises with fusion to yield the best overall accuracy.

Table 2: Noise-free Euclidean  $RMSE_{xy}$  (metres) on the held-out test sets.

Variant	Dataset 1	Dataset 2
PF + RF	1.00	0.68
PF + RF + KNN + DST	0.80	0.55
PF + PH + RF	0.99	0.68
PF + PH + RF + KNN + DST	0.44	0.32

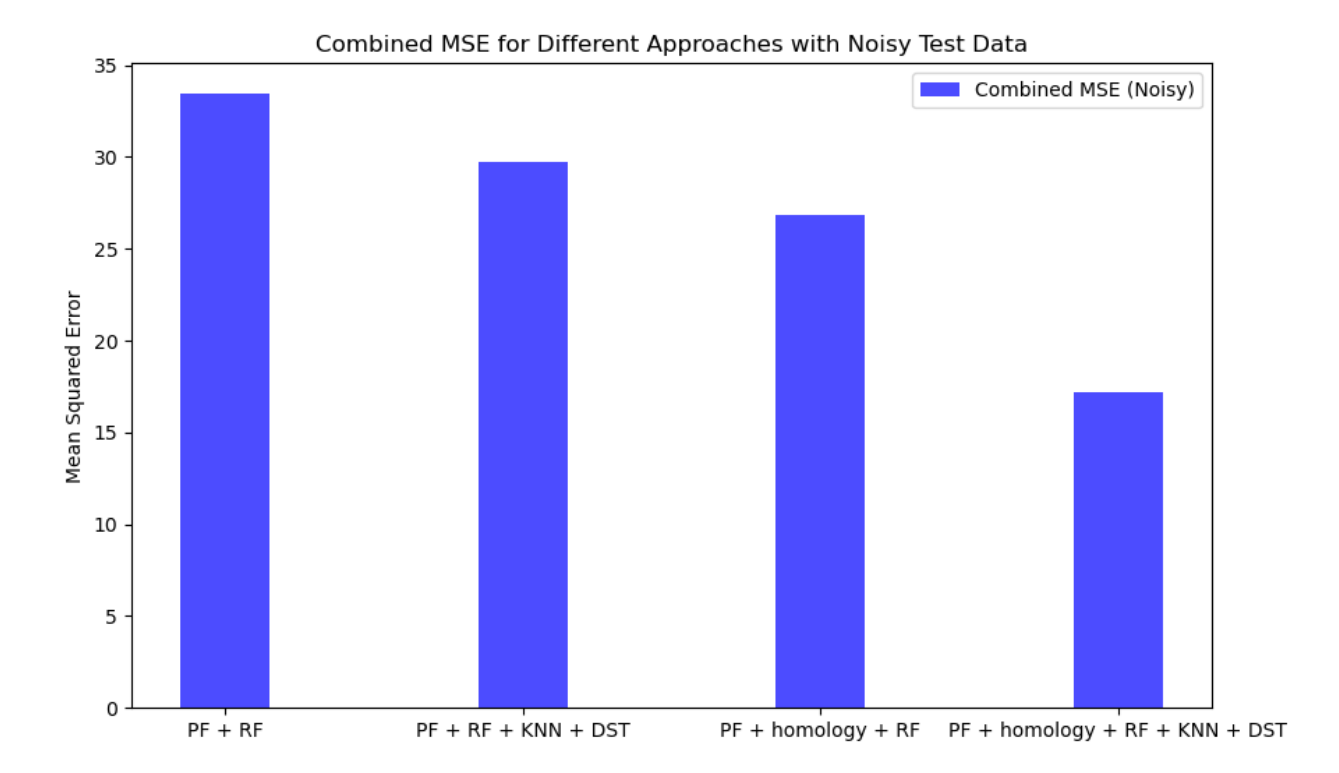


Figure 10: Dataset 1 — 10% Gaussian RSS perturbation. Layer-by-layer ablation shows cumulative gains from filtering, DST fusion method, and PH.

All claims are backed by ablations, cross-dataset replication, and significance tests. In this paper, we distinguish noise-free setting and also noisy settings to avoid over-claiming performance in our research.

# 3.13 Threats to Validity

Our datasets are medium-scale and site-specific; broader generalisation requires additional buildings and devices. The injected noise model is Gaussian; real-world interference can be bursty or device-dependent. Finally, PF latency may exceed tight real-time constraints; the KF variant addresses this with a small accuracy trade-off.

## 4 Conclusion and Future Work

We presented a topology-aware, hybrid Wi-Fi/BLE fingerprinting framework that combines physically consistent RSS normalisation, classical Bayesian denoising (KF/UKF/PF), complementary regressors (RF and weighted kNN), and principled fusion via Dempster–Shafer theory with a two-source Choquet integral, augmented by per-sample persistent-homology features. The system produces both point (x, y) estimates and interpretable belief maps, and is engineered for embedded deployment. Across two heterogeneous datasets, the full pipeline offers consistent gains over a strong PF+RF baseline: under 10% synthetic RSS noise it attains 3.40 m (Dataset 1) and 2.45 m (Dataset 2) RMSE $_{xy}$ —an average improvement of about 37%—while in noise-free conditions it reaches 0.44 m and 0.32 m, up to 56% better. Over ten stratified splits with the same noise protocol, the mean is  $4.993 \pm 0.15$  m versus  $6.292 \pm 0.13$  m for PF+RF

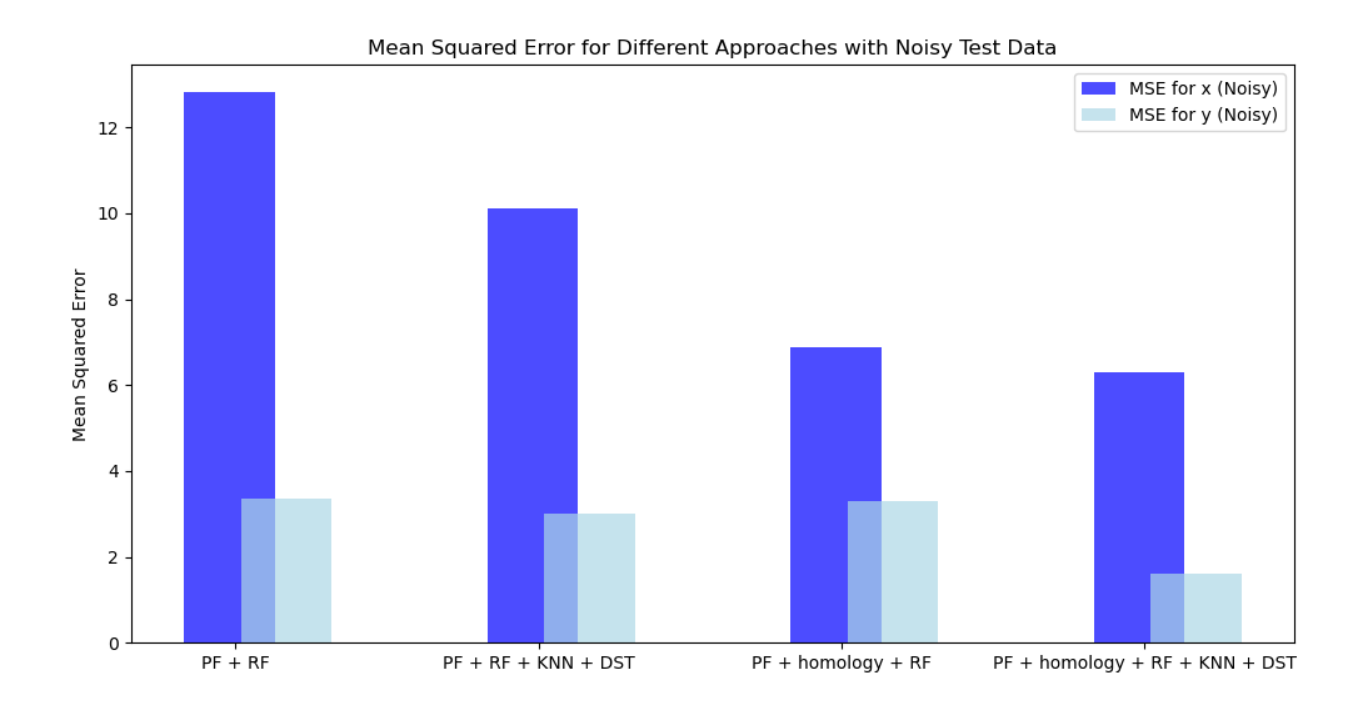


Figure 11: Dataset 2 — 10% RSS noise.

Table 3: Per-dataset RMSE<sub>xy</sub> (m) under **10% test-only Gaussian RSS noise** (in dBm,  $\sigma_i = 0.10 \times$  training-set std for channel i); **canonical held-out split**. Same noise setting is used in Figs. 10–11.

Variant	Dataset 1	Dataset 2
PF + RF	5.426	3.886
PF + RF + KNN + DST	5.196	3.529
PF + PH + RF	5.380	3.733
PF + PH + RF + KNN + DST	3.397	2.448

with p < 0.001, confirming statistical significance. Compared with lightweight Wi-Fi-only baselines, the hybrid design roughly halves error through multi-radio sensing, complementary regressors, and evidence-theoretic fusion; relative to deep models, it trades a small amount of headline accuracy for robustness under noise and *microcontroller-class* deployability—our KF variant operates in real time on ESP32-class devices, while PF further improves accuracy at higher latency.

Looking ahead, we will pursue calibration-free adaptation across devices to mitigate RSS offsets; richer sensing and tighter filtering by fusing inertial, magnetic, and barometric cues (e.g., Rao–Blackwellised PF or factor-graph smoothing) for trajectory and floor inference; robust noise modelling with heavy-tailed/bursty likelihoods and online scale learning; learning the fusion layer to move from grid-based DST to continuous belief fields while preserving interpretability; topology-aware graph modelling over RP graphs; efficiency auto-tuning of  $M_p$ , k, and RF depth under latency/energy constraints with on-device profiling; multi-building, multi-device studies with unified noise/runtime benchmarks and archival artifacts; and privacy-preserving radio-map construction via on-device aggregation or federated updates—alongside releasing open-source implementations, datasets, and evaluation scripts to enable reproducibility and community benchmarking; and formal uncertainty calibration (e.g., reliability diagrams, expected calibration error) with conformal prediction for actionable confidence intervals.

#### References

[1] F. Zafari, A. Gkelias, and K. K. Leung, "A survey of indoor localization systems and technologies," *IEEE Commun. Surv. Tut.*, vol. 21, no. 3, pp. 2568–2599, 2019.

Table 4: Mean RMSE<sub>xy</sub> with 95% confidence intervals across 10 stratified splits under the same 10% noise definition as Table 3. Relative improvement is  $100 \times (PF+RF - Ours)/PF+RF = 20.6\%$ .

Method	$\mathrm{RMSE}_{xy}\left(\mathbf{m}\right)$
PF + RF	$6.292 \pm 0.13$
PF + RF + KNN + DST	$5.468 \pm 0.14$
PF + PH + RF	$5.690 \pm 0.16$
PF + PH + RF + KNN + DST	$\boldsymbol{4.993 \pm 0.15}$

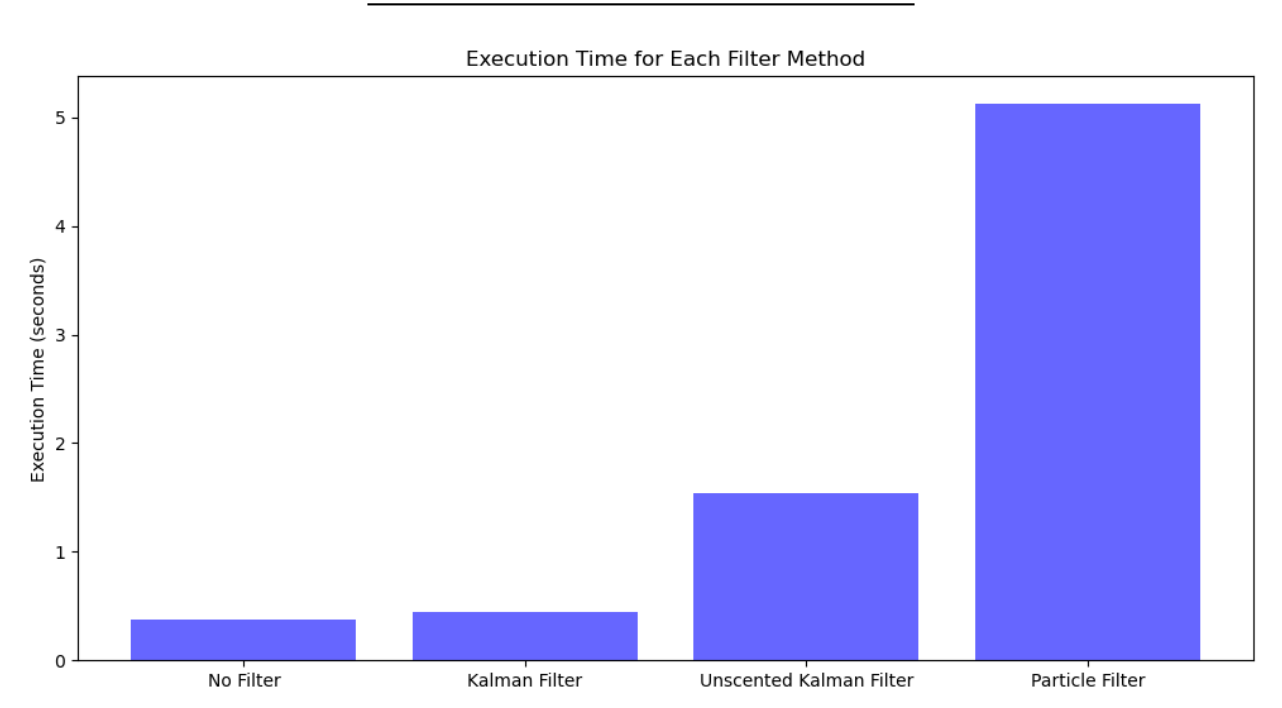


Figure 12: Per-update latency on Dataset 1 (hardware: ESP32-class MCU). The KF-based pipeline is real-time; PF increases latency by roughly an order of magnitude.

- [2] A. Sesyuk, S. Ioannou, and M. Raspopoulos, "A survey of 3D indoor localization systems and technologies," *Sensors*, vol. 22, no. 23, Art. ID 9380, 2022.
- [3] J. Rezaie, B. Moshiri, B. N. Araabi, and A. Asadian, "GPS/INS integration using nonlinear blending filters," in *Proc. SICE 2007 Annu. Conf.*, 2007, pp. 1674–1680.
- [4] M. Jafari, M. Sahebjameyan, B. Moshiri, and T. A. Najafabadi, "Skew redundant MEMS IMU calibration using a Kalman filter," *Meas. Sci. Technol.*, vol. 26, no. 10, Art. ID 105002, 2015.
- [5] A. Vafamand, B. Moshiri, and N. Vafamand, "Fusing unscented Kalman filter to detect and isolate sensor faults in DC microgrids with CPLs," *IEEE Trans. Instrum. Meas.*, vol. 71, Art. ID 7008611, 2021.
- [6] Y. Leng, F. Huang, and W. Tan, "A Wi-Fi fingerprint positioning method based on SLWKNN," *IEEE Sensors J.*, early access, 2024.
- [7] S. C. Narasimman and A. Alphones, "*DumbLoc*: Dumb indoor localization framework using Wi-Fi fingerprinting," *IEEE Sensors J.*, early access, 2024.
- [8] B. Hou and Y. Wang, "RF-KELM indoor positioning algorithm based on Wi-Fi RSS fingerprint," *Meas. Sci. Technol.*, vol. 35, no. 4, Art. ID 045004, 2024.
- [9] C. Wang, Z. Yang, *et al.*, "*DLoc*: Precise indoor localization with deep neural mapping and commodity WiFi," in *Proc. ACM MobiCom*, 2020, pp. 1–13.
- [10] Y. Zhang, H. Li, and X. Wei, "CSI trajectory fingerprinting with GAN-augmented CNN-LSTM," *IEEE Trans. Mobile Comput.*, vol. 20, no. 12, pp. 3402–3416, 2021.

Table 5: Comparison with recent Wi-Fi / Wi-Fi+BLE fingerprinting methods.

Method	Modality / Model	RMSE (m)
RLWKNN [6]	Wi-Fi / Range-limited KNN	4.8
DumbLoc [7]	Wi-Fi / Heuristic matching	6.2
RF-KELM [8]	Wi-Fi / Kernel ELM	3.9
SPOTTER [13]	Wi-Fi+BLE / Particle Filter	2.7
HoGNNLoc [14]	Wi-Fi / GNN	1.8
DLoc [9]	Wi-Fi / CNN+LSTM	1.2
This work	Wi-Fi+BLE / PF+RF+KNN+DST+PH	3.40 / 2.45 <sup>†</sup>

<sup>&</sup>lt;sup>†</sup> Dataset 1 / Dataset 2 with 10% synthetic noise. External works typically report noise-free results; absolute values are not directly comparable.

- [11] C. Belmonte-Fernández, F. J. García-Pardo, and L. Valcarce, "Generative hidden-Markov Wi-Fi fingerprinting with sub-meter accuracy," *IEEE Sensors J.*, vol. 21, no. 18, pp. 20882–20894, 2021.
- [12] J. Xia, et al., "Optimization of Fingerprint Matching Localization Algorithm Based on RSSI in Wireless Sensor Network," IEEE Sensors J., 2025.
- [13] M. Azaddel, S. Kiani, and D. Burdakis, "SPOTTER: Particle-filter fusion of Wi-Fi and BLE for accurate indoor positioning," in *Proc. IEEE PerCom*, 2023, pp. 1–10.
- [14] Q. Kang, H. Wang, and Z. Ding, "HoGNNLoc: High-order graph neural network for Wi-Fi fingerprint localization," in *Proc. IEEE INFOCOM*, 2023, pp. 2144–2152.
- [15] A. Moradbeikie, E. Ghobadi, and M. Bagherzadeh, "RSSI-based localization in industrial environments: A Wi-Fi/BLE hybrid approach," in *Proc. IEEE Int. Conf. Industrial Technology (ICIT)*, 2024, pp. 861–866.
- [16] J. O. Ogutu, H. P. Piepho, and T. Schulz-Streeck, "A comparison of random forests, boosting and support vector machines for genomic selection," *BMC Proc.*, vol. 5, suppl. 3, S11, 2011.
- [17] D. Maulud and A. M. Abdulazeez, "A review on linear regression comprehensive in machine learning," *J. Appl. Sci. Technol. Trends*, vol. 1, no. 2, pp. 140–147, 2020.
- [18] S. Konatowski, P. Kaniewski, and J. Matuszewski, "Comparison of estimation accuracy of EKF, UKF and PF filters," *Annual of Navigation*, vol. 23, pp. 69–87, 2016.
- [19] K. Sentz and S. Ferson, "Combination of evidence in Dempster–Shafer theory," Sandia Nat. Lab., Tech. Rep. SAND2002-0835, 2002.
- [20] T. Murofushi and M. Sugeno, "Fuzzy measures and fuzzy integrals," in *Fuzzy Measures and Integrals: Theory and Applications*, Heidelberg: Physica-Verlag, 2000, pp. 3–41.
- [21] G. Carlsson, "Topology and data," Bull. Amer. Math. Soc., vol. 46, no. 2, pp. 255–308, 2009.
- [22] R. HoseinNezhad, B. Moshiri, and M. R. Asharif, "Sensor fusion for ultrasonic and laser arrays in mobile robotics: a comparative study of fuzzy, Dempster and Bayesian approaches," in *Proc. IEEE SENSORS*, 2002, vol. 2, pp. 1682–1689.
- [23] E. Kazemi, D. S. Zadeh, and B. Moshiri, "Metal-oxide-semiconductor sensors modeling using ordered weighted averaging (OWA) operators in electronic nose," *Measurement*, vol. 184, Art. ID 109932, 2021.